View metadata, citation and similar papers at core.ac.uk
brought to you by CORE
provided by Chalmers Publication Library

JOURNAL OF GEOPHYSICAL RESEARCH, VOL. 115, B03407, doi:10.1029/2009JB006579, 2010

Click Here for Full Article

Impact of atmospheric turbulence on geodetic very long baseline interferometry

T. Nilsson[1,2] and R. Haas[1]

Received 29 April 2009; revised 1 October 2009; accepted 27 October 2009; published 12 March 2010.

[1] We assess the impact of atmospheric turbulence on geodetic very long baseline interferometry (VLBI) through simulations of atmospheric delays. VLBI observations are simulated for the two best existing VLBI data sets: The continuous VLBI campaigns CONT05 and CONT08. We test different methods to determine the magnitude of the turbulence above each VLBI station, i.e., the refractive index structure constant C_n^2. The results from the analysis of the simulated data and the actually observed VLBI data are compared. We find that atmospheric turbulence today is the largest error source for geodetic VLBI. Accurate modeling of atmospheric turbulence is necessary to reach the highest accuracy with geodetic VLBI.

Citation: Nilsson, T., and R. Haas (2010), Impact of atmospheric turbulence on geodetic very long baseline interferometry, *J. Geophys. Res.*, *115*, B03407, doi:10.1029/2009JB006579.

1. Introduction

[2] Radio signals are delayed in the neutral atmosphere of the Earth. This delay is an important error source for space geodetic techniques, such as Global Navigation Satellite Systems (GNSS) and geodetic very long baseline interferometry (VLBI). We need to correct for the atmospheric delay in order to obtain the most accurate results with these techniques. Generally, the atmospheric delay is divided into two parts: one hydrostatic delay and one wet delay. The hydrostatic delay can be estimated using measurements of the atmospheric pressure at the surface. The wet delay can, however, not be estimated with high accuracy from surface measurements.

[3] In VLBI mainly two methods exist to correct for the wet delay. The first one is to use an independent instrument, such as a water vapor radiometer (WVR), for estimating the atmospheric delay [*Elgered et al.*, 1991; *Kuehn et al.*, 1991; *Emardson et al.*, 1999]. However, these estimates also contain errors, e.g., calibration errors and uncertainties in the conversion from measured brightness temperatures to atmospheric delays. Furthermore, a WVR does not give reliable results during rain.

[4] The other method is to estimate the wet atmospheric delays along with the other parameters normally estimated in the VLBI data analysis, such as the station coordinates, clock errors, and Earth orientation parameters. This approach requires a model that describes the atmospheric delay as a function of observation direction and time. Typically, it is modeled as the delay in the zenith direction times a mapping function plus linear horizontal gradients [*MacMillan*, 1995]. This model assumes that the refractive index of air has only linear variations in the horizontal direction. The temporal variations in the model parameters are described either by piecewise linear functions (analysis based on classical least squares method [e.g., *Ma et al.*, 1990]) or by random walk processes (analysis based on Kalman filtering [e.g., *Herring et al.*, 1990]). However, such a model does not describe the small-scale fluctuations in the atmosphere caused by turbulence, since these are not linear.

[5] The two methods give similar accuracy in the VLBI results [*Emardson et al.*, 1999] despite problems to estimate wet atmospheric delays from WVR data observed during rain. There are two reasons for not achieving better results when estimating the atmospheric delay in the VLBI analysis compared to using an external calibration. The first one is increased sensitivity to noise since more parameters need to be estimated in the analysis. The other is that atmospheric turbulence is not represented in the atmospheric delay model used in the data analysis.

[6] Here we present simulations designed to investigate the errors in the VLBI results due to atmospheric turbulence. We do this by simulating VLBI observations for the CONT05 and CONT08 campaigns (section 2), which are the two best existing VLBI data sets, using a method based on the theory of atmospheric turbulence (section 3). For the simulations we need the refractive index structure constant C_n^2, a parameter which in principle describes the magnitude of the turbulent variations. Several methods for estimating this parameter are presented in section 4. The simulation setup and the processing of the simulated and the actually observed VLBI data are described in section 5. The results and the conclusions are presented in sections 6 and 7, respectively.

2. CONT05 and CONT08 Campaigns

[7] CONT05 and CONT08 are two VLBI campaigns, each consisting of 15 days of continuous observations, observed 12–27 September 2005 and 12–26 August 2008, respectively. Each campaign consisted of 15 one day ses-

[1]Onsala Space Observatory, Department of Radio and Space Science, Chalmers University of Technology, Onsala, Sweden.
[2]Now at Institute of Geodesy and Geophysics, Vienna University of Technology, Vienna, Austria.

Copyright 2010 by the American Geophysical Union.
0148-0227/10/2009JB006579

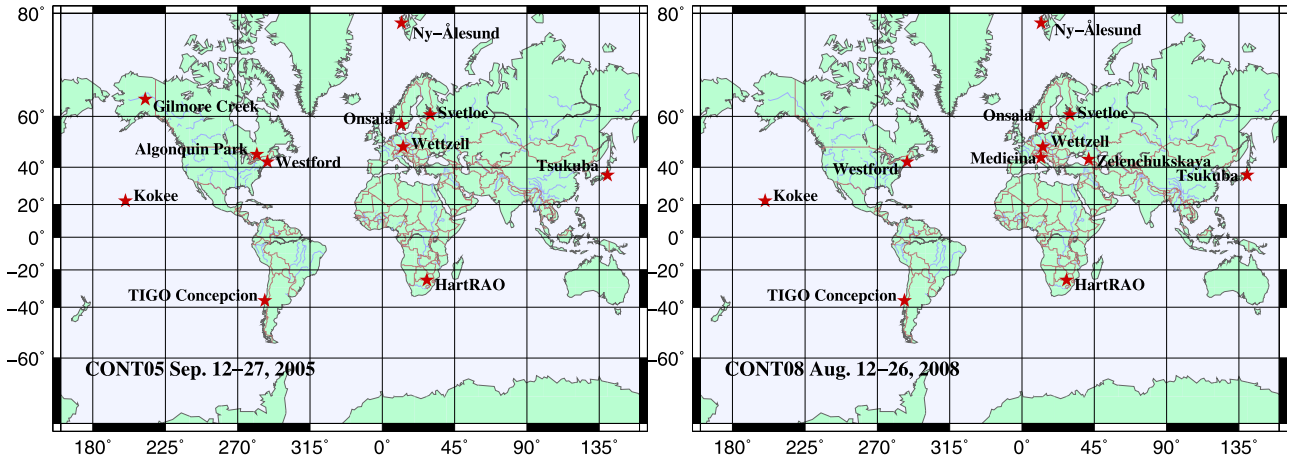

Figure 1. The locations of the stations in (left) CONT05 and (right) CONT08.

sions. Eleven VLBI stations participated in each campaign, of which nine were in both (see Figure 1).

[8] Table 1 gives information about the station locations, the average number of scans observed at each station per day, the average number of stations involved in a scan, and the average number of unique radio sources observed by each station per day. As seen, there were more observations in CONT08 than in CONT05. This is because of shorter scans in CONT08 made possible by a higher data acquisition rate (512 Mbit s^{-1} compared to 256 Mbit s^{-1} in CONT05).

3. Theory

[9] In this section we review the method for simulating atmospheric delays in a turbulent atmosphere [*Nilsson et al.*, 2007; *Nilsson and Haas*, 2008]. Since turbulence affects both the wet and the hydrostatic parts of the total delays, we simulate the total delays. The slant total delay ℓ_i of a radio signal observed at time t_i is given by

$$\ell_i = \int_{S_i} [n(\mathbf{r}_i(s)) - 1]\, ds, \tag{1}$$

where S_i is the slant path of the signal and $n(\mathbf{r})$ is the refractive index at position $\mathbf{r}$. The refractive index can be expressed as a function of the atmospheric pressure P, temperature T, and the partial pressure of water vapor e [*Elgered*, 1993]:

$$n = 1 + 10^{-6}\left[k_1 \frac{P}{T} + k_2' \frac{e}{T} + k_3 \frac{e}{T^2}\right], \tag{2}$$

where k_1, k'_2, and k_3 are constants.

[10] When simulating atmospheric delays it is convenient to use the slant delay mapped to the zenith direction, the equivalent zenith delay ℓ_i^z:

$$\ell_i^z = \frac{1}{m_i}\int_S [n(\mathbf{r}_i(s)) - 1]\, ds = \int_0^\infty [n(\mathbf{r}_i(z)) - 1]\, dz, \tag{3}$$

where $m_i = m(\epsilon_i)$ is the mapping function between elevation angle ϵ_i and zenith. Typically, the mapping function is divided into two parts, one for the hydrostatic delay and one for the wet delay. Although turbulence of course causes fluctuations in both the wet and the hydrostatic delays, the fluctuations in the wet delay are typically a magnitude larger then those in the hydrostatic delay [*Hill et al.*, 1988]. Hence,

Table 1. Information About the Stations and the Observation Schedules of the Two CONT Campaigns

			CONT05			CONT08		
Station	Latitude (°N)	Longitude (°E)	Number of Scans per Day	Number of Stations per Scan	Number of Sources per Day	Number of Scans per Day	Number of Stations per Scan	Number of Sources per Day
Algonquin Park	46	−78	161.5	5.4	43.0	–	–	–
Gilmore Creek	65	−147	448.8	4.7	49.7	–	–	–
HartRAO	−26	28	239.4	4.1	34.1	334.2	4.7	38.3
Kokee Park	22	−160	406.9	3.8	61.5	657.9	3.7	73.5
Medicina	45	12	–	–	–	476.1	6.3	58.5
Ny-Ålesund	79	12	366.3	5.6	41.7	532.2	5.8	41.3
Onsala	57	12	314.1	5.7	46.1	480.1	6.6	48.3
Svetloe	61	30	356.6	5.5	50.3	480.5	6.5	52.3
TIGO Concepcion	−37	−73	173.5	2.7	20.9	360.7	2.9	39.7
Tsukuba	36	140	443.6	4.2	63.9	640.5	4.3	72.9
Westford	43	−71	334.9	5.0	51.9	492.9	5.1	54.1
Wettzell	49	13	307.4	5.5	51.1	500.9	6.4	57.9
Zelenchukskaya	44	42	–	–	–	360.7	6.5	54.5
Total	–	–	920.0	3.9	68.3	1314.5	4.0	78.0

we here use the wet mapping function of *Niell* [1996] for the fluctuating part of the total delay.

[11] In the presence of turbulence we can divide the refractive index into two parts, $n = \overline{n} + \delta n$, where $\overline{n}$ is the mean (nonturbulent) part and δn is the fluctuating (turbulent) part. Thus, ℓ_i^z can also be written as a mean part $\overline{\ell}_i^z$ plus a fluctuating part $\delta\ell_i^z$:

$$\ell_i^z = \int_0^\infty [\bar{n}(\mathbf{r}_i(z)) - 1]\,dz + \int_0^\infty [\delta n(\mathbf{r}_i(z)) - 1]\,dz = \overline{\ell}_i^z + \delta\ell_i^z. \tag{4}$$

Most of the small-scale variations in ℓ_i^z will be caused by turbulence, i.e., the variations in $\delta\ell_i^z$. Variations in the mean part $\overline{\ell}_i^z$ are typically occurring slowly (timescales of several hours and more) and over large distances (>100 km). These are caused by, e.g., passages of weather fronts and evaporation/condensation of water vapor. We are mainly interested in the variations caused by turbulence; hence we will, for simplicity, assume that the mean part is constant. The changes in the mean part should be modeled very well by the atmospheric model used in the VLBI analysis and thus will not cause any large errors in the VLBI results.

[12] We want to simulate a series of N equivalent zenith delays: $\ell_0^z, \ell_1^z, \ell_2^z, \ldots, \ell_{N-1}^z$. We choose one of these, e.g., ℓ_0^z, as a reference and consider the difference between the other equivalent zenith delays and this one. We then calculate the covariance matrix C, where the (i, j)th component is [*Nilsson et al.*, 2007]

$$\begin{aligned} C_{ij} &= \langle (\delta\ell_i^z - \delta\ell_0^z)(\delta\ell_j^z - \delta\ell_0^z)\rangle \\ &= \frac{1}{2}\int_0^\infty \int_0^\infty \Big[\langle [\delta n(\mathbf{r}_i(z), t_i) - \delta n(\mathbf{r}_0(z'), t_0)]^2\rangle \\ &\quad + \langle [\delta n(\mathbf{r}_j(z), t_j) - \delta n(\mathbf{r}_0(z'), t_0)]^2\rangle \\ &\quad - \langle [\delta n(\mathbf{r}_i(z), t_i) - \delta n(\mathbf{r}_j(z'), t_j)]^2\rangle \\ &\quad - \langle [\delta n(\mathbf{r}_0(z), t_0) - \delta n(\mathbf{r}_0(z'), t_0)]^2\rangle\Big]\,dz\,dz'. \end{aligned} \tag{5}$$

According to the theory of Kolmogorov turbulence, the structure function for the refractive index fluctuations is [*Tatarskii*, 1971; *Treuhaft and Lanyi*, 1987]

$$\langle [\delta n(\mathbf{r}_i) - \delta n(\mathbf{r}_j)]^2\rangle = C_n^2(z_i, z_j)\,\frac{\| \mathbf{r}_i - \mathbf{r}_j \|^{2/3}}{1 + \dfrac{\| \mathbf{r}_i - \mathbf{r}_j \|^{2/3}}{L^{2/3}}}, \tag{6}$$

where C_n^2 is called the refractive index structure constant, z_i is the vertical component of $\mathbf{r}_i$, and L is the saturation length scale (needed to avoid infinite variations at infinite distances). This equation, however, only gives the spatial variations in δn. If we assume that the temporal variations are caused by the air moving with the wind (Taylor's frozen flow hypothesis [*Taylor*, 1938]), then $\delta n(\mathbf{r}, t) = \delta n(\mathbf{r} - \mathbf{v}(t - t_0), t_0)$, where $\mathbf{v}$ is the wind velocity. This approximation is not valid for variations over long time periods, but should work reasonably well for short time variations (less than a few hours), which are of interest in this work. Hence, for spatial and temporal variations we have

$$\langle [\delta n(\mathbf{r}_i, t_i) - \delta n(\mathbf{r}_j, t_j)]^2\rangle = C_n^2(z_i, z_j)\,\frac{\| \mathbf{r}_i - \mathbf{r}_j - \mathbf{v}(t_i - t_j) \|^{2/3}}{1 + \dfrac{\| \mathbf{r}_i - \mathbf{r}_j - \mathbf{v}(t_i - t_j) \|^{2/3}}{L^{2/3}}}. \tag{7}$$

Thus, if C_n^2, L, and $\mathbf{v}$ are known, it is possible to calculate the covariance matrix C given by equation (5). It is then possible to simulate $\boldsymbol{\delta\ell} = [\delta\ell_1^z, \ldots, \delta\ell_{N-1}^z]^T$ simply by generating a series of $N - 1$ random numbers with covariance matrix C. In order to do this, we need to know the distribution of $\boldsymbol{\delta\ell}$. A simple case (which is a good approximation) is to assume a Gaussian distribution. In that case, we make a Cholesky factorization [*Press et al.*, 1992] of C

$$C = D\,D^T \tag{8}$$

and obtain simulated values for $\boldsymbol{\delta\ell}$ by

$$\boldsymbol{\delta\ell} = \delta\ell_0^z + D\mathbf{w}, \tag{9}$$

where $\mathbf{w}$ is a vector of zero mean Gaussian random numbers with variance one. Then the simulated $\boldsymbol{\ell}^z = [\ell_1^z, \ell_2^z, \ldots, \ell_{N-1}^z]^T$ will be obtained by (assuming $\overline{\ell}_i^z = \overline{\ell}^z$ to be constant)

$$\ell^z = \overline{\ell}^z + \boldsymbol{\delta\ell} = \overline{\ell}^z + \delta\ell_0^z + D\mathbf{w} = \ell_0^z + D\mathbf{w}. \tag{10}$$

A value for ℓ_0^z can be chosen freely, like a typical value for the zenith delay. Finally, in order to obtain the slant delays, the equivalent zenith delays are mapped to the slant direction by multiplying with the mapping function.

[13] For the simulations we need to know a number of parameters: the structure constant C_n^2, the saturation length scale L, the wind velocity $\mathbf{v}$, and ℓ_0^z. As stated above, ℓ_0^z can be chosen as a typical value of the zenith delay. In this work we use 20 cm for all stations. The value used should not have any effect on the simulation results. The same is true for the value of L, since the effect of L will only be seen at large scales (given that L is large). We use L = 3000 km, as used by *Treuhaft and Lanyi* [1987]. The wind velocity can be obtained, e.g., from numerical weather prediction models. We use a wind velocity constant with height and equal to the wind at the 850 hPa level obtained from European Centre for Medium Range Weather Forecasts (ECMWF) analysis data. The 850 hPa level (1400–1500 m altitude) corresponds approximately to the mean height of the atmospheric water vapor; thus, the wind at this level is a good choice for the wind to be used in the simulations. Methods for estimating C_n^2, as well as some published values, are presented in section 4.

4. Methods for Estimating C_n^2

4.1. Radar Measurements

[14] One way to estimate a C_n^2 profile is to use Doppler radar measurements. The power backscattered from a spe-

cific height is due to the irregularities caused by turbulence at that height. According to *Ottersten* [1969], the radar reflectivity η for clear air is related to C_n^2 through the expression

$$\eta = 0.38\, C_n^2 \lambda^{-1/3}, \tag{11}$$

where λ is the radar wavelength. According to *Nastrom et al.* [1986], the C_n^2 values determined from the radar should be accurate within a factor of 2.

[15] There exist a number of investigations where C_n^2 is measured with radars, although there are not many that present time series of C_n^2 in the lower troposphere from longer time periods (months to years). *Chadwick and Moran* [1980] presented 1 year of measurements of C_n^2 in Colorado. They found that the median value of C_n^2 at 805 m altitude varied from about 10^{-15} m$^{-2/3}$ in May–June to below 10^{-16} m$^{-2/3}$ in November. The observed values at this height were very variable, with occasional values larger than 10^{-13} m$^{-2/3}$. It was also shown that C_n^2 had a lognormal distribution and that $\log(C_n^2)$ had a standard deviation of about 6 dB. Hence, the mean C_n^2 should be larger than the median ones by a factor of roughly 2.5.

[16] *Nastrom et al.* [1986] and *Rao et al.* [1997, 2001] used radar data to study the seasonal variations in C_n^2. They all found that C_n^2 generally is larger in summer than in winter. However, all these studies concentrated on higher altitudes (>4 km) where C_n^2 generally is much smaller than at lower altitudes.

[17] Other investigations have focused on shorter periods (a few days). *Heo et al.* [2003] showed estimated C_n^2 between 0 and 2.5 km above Viabon, France, for 2 days in June 1998. They found C_n^2 values ranging from 10^{-15} up to 10^{-12} m$^{-2/3}$, with most of the values being between 10^{-14} and 10^{-13} m$^{-2/3}$. In the various C_n^2 profiles presented by *Cohn* [1995], *Hocking and Mu* [1997], *Luce et al.* [1997], and *Zink et al.* [2004], C_n^2 is around 10^{-14} m$^{-2/3}$ at altitudes of 1–2 km.

4.2. Radiosonde Data

[18] It is possible to estimate C_n^2 using profiles of atmospheric pressure, temperature, humidity, and wind speed. Assuming that the small-scale fluctuations in the refractive index are created by turbulent mixing of large-scale refractive index variations, we can express C_n^2 as [*VanZandt et al.*, 1978; *d'Auria et al.*, 1993]

$$C_n^2 = a^2\, F\, L_0^{4/3}\, M^2, \tag{12}$$

where $a^2 \approx 2.8$, L_0 is the outer scale of atmospheric turbulence (proportional to the turbulence "mixing length"), M is the potential refractive index gradient, and F is called the intermittency factor expressing the fraction of the air that is turbulent. The potential refractive index gradient can be approximated by the gradient in the vertical direction since the vertical variations in the refractive index typically are much (more than 10 times) larger than those in the horizontal direction. This gradient includes only the part of the vertical gradient of n caused by the vertical gradients in quantities conserved under adiabatic motion, i.e., the potential temperature θ and the specific humidity q:

$$\theta = T\left(\frac{P_0}{P}\right)^{0.286} \tag{13}$$

$$q = \frac{e}{1.62\, P}, \tag{14}$$

where P_0 = 1000 hPa. Since the specific humidity is a conserved quantity only for cloud-free conditions, this method cannot be used when clouds are present.

[19] Using equation (2) for the refractive index, we get

$$\begin{aligned} M &= \frac{\partial \overline{n}}{\partial \overline{\theta}}\frac{\partial \overline{\theta}}{\partial z} + \frac{\partial \overline{n}}{\partial \overline{q}}\frac{\partial \overline{q}}{\partial z} \\ &= -10^{-6}\frac{P}{T}\left[\left(k_1 + 1.62\, k_2' q + 3.24\, k_3 \frac{q}{T}\right)\frac{1}{\overline{\theta}}\frac{\partial \overline{\theta}}{\partial z}\right. \\ &\quad \left. - \left(1.62\, k_2' + 1.62\, \frac{k_3}{T}\right)\frac{\partial \overline{q}}{\partial z}\right]. \end{aligned} \tag{15}$$

The intervals over which the vertical gradients in θ and q are calculated should be much larger than L_0 since these are the gradients in the mean quantities and should not contain any turbulence. Here we calculate M over intervals of 500 m.

[20] The outer scale L_0 is generally unknown and can vary from less than 1 up to 100 m or more [*d'Auria et al.*, 1993]. Typically, this problem is solved by assuming a statistical distribution for L_0 and replacing L_0 in equation (12) by $L_{0\mathrm{eff}} = \langle L_0^{4/3} \rangle^{3/4}$. Often L_0 is assumed to be uniformly distributed between $L_{0\min}$ and $L_{0\max}$. According to *d'Auria et al.* [1993], $L_{0\min}$ is in the range of 0.1–5 m and $L_{0\max}$ is in the range of 30–100 m. Here we assume $L_{0\min}$ = 3 m and $L_{0\max}$ = 70 m, i.e., approximately the midvalues of the given ranges. Using $L_{0\max}$ = 100 m instead of 70 m will cause C_n^2 to be larger by approximately a factor of 1.6.

[21] The intermittency factor F is required since not all of the atmosphere is turbulent. This factor can vary between 0 and 1, typically $F \approx 0.1$ [*VanZandt et al.*, 1978]. In this work, we have calculated F using the Richardson number Ri:

$$Ri = \frac{g}{\theta}\frac{\partial \theta}{\partial z}\left\|\frac{\partial \mathbf{v}}{\partial z}\right\|^{-2}. \tag{16}$$

One simple way to calculate F would be to let F = 1 when Ri is less than the critical Richardson number $Ri_c \approx 0.25$, and F = 0 otherwise. We have used a slightly more advanced model for calculating F which gives a more smooth behavior of F around $Ri = Ri_c$ [*d'Auria et al.*, 1993; *Vasseur*, 1999]:

$$F = \int_{S_c}^{\infty} p(S)\, dS, \tag{17}$$

where $S = \|\partial \mathbf{v}/\partial z\|$, S_c is the value of S that makes $Ri = Ri_c$, and $p(S)$ is the probability density function for S (assumed to be that of a Rice distribution; see *d'Auria et al.* [1993] for details).

[22] Figure 2 shows C_n^2 profiles obtained using high-resolution radiosonde data from Herstmonceux and St. Helena.

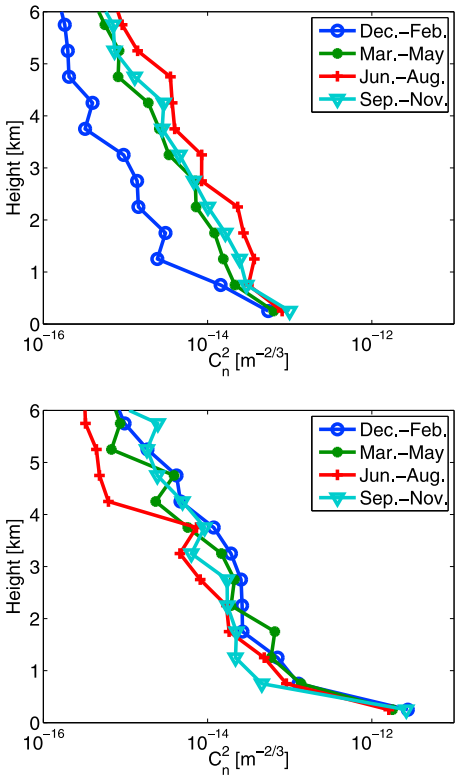

Figure 2. Mean C_n^2 profiles of different seasons for (top) Herstmonceux and (bottom) St. Helena. The station locations are listed in Table 2.

Shown are the mean profiles obtained from 2003–2006 and for different seasons: December-February, March-May, June-August, and September-November. We note that C_n^2 is generally larger in the summer compared to the winter.

[23] Table 2 shows the estimated parameters C_{n0}^2 and H for five radiosonde stations. These parameters were obtained from a fit of mean profiles of the different seasons to the model:

$$C_n^2(z) = C_{n0}^2 \exp\left[-\frac{2z}{H}\right]. \tag{18}$$

We note that the low latitude sites generally give higher C_n^2 values than the high latitude sites.

[24] Unfortunately, high-resolution radiosonde data are not commonly available at the VLBI station locations. Thus, in order to obtain C_n^2 values for the VLBI stations in CONT05 and CONT08 we have used the radiosonde profiles of Table 2 which are closer in latitude. The station specific parameters are given in Table 3.

Table 3. Station Specific C_n^2 Values for CONT05 and CONT08 Obtained From Radiosonde Data and From the 24 h Variance of the Zenith Total Delay Observed by GPS[a]

	CONT05				CONT08			
	Radiosonde		GPS		Radiosonde		GPS	
			C_n^2				C_n^2	
Station	C_n^2	H	Const	Exp	C_n^2	H	Const	Exp
Algonquin Park	2.26	2518	11.33	11.69	–	–	–	–
Gilmore Creek	1.24	3114	0.96	0.99	–	–	–	–
HartRAO	1.65	3207	2.17	2.24	1.98	1702	2.58	2.70
Kokee Park	2.39	2804	3.18	3.27	2.33	3625	3.36	3.47
Medicina	–	–	–	–	2.84	2659	8.09	8.44
Ny-Ålesund	1.34	3114	0.91	0.96	1.03	4232	1.22	1.27
Onsala	1.35	3114	4.37	4.50	1.03	4232	3.10	3.20
Svetloe	1.34	3114	2.40	2.47	1.03	4232	6.85	7.06
TIGO Concepcion	2.44	3207	2.32	2.40	4.10	1702	4.33	4.47
Tsukuba	3.52	2804	5.30	5.47	3.15	3625	16.12	16.78
Westford	3.52	2804	13.44	13.84	3.15	3625	9.72	10.09
Wettzell	1.89	2518	3.24	3.34	2.27	2659	5.43	5.65
Zelenchukskaya	–	–	–	–	1.87	2659	9.95	10.39

[a]For the latter case, the displayed values are obtained when assuming a constant C_n^2 up to 2 km (Const) and when assuming the C_n^2 profile described by equation (22) (Exp, the values shown are C_n^2 at the surface). The units of the C_n^2 and H values are 10^{-14} m$^{-2/3}$ and m, respectively.

[25] *Vasseur* [1999] presented a mean C_n^2 profile obtained from 1 year of radiosonde data from Uccle, Belgium, which is similar to those obtained here for the station Lerwick ($C_n^2 \sim 10^{-14}$ m$^{-2/3}$ at 1–2 km altitude). Similar results were also obtained by *Ravard and Chevrier* [1996] using radiosonde data from four radiosonde stations in France. They also noted that C_n^2 for lower altitudes seemed to be larger for the radiosonde sites close to the sea compared to the inland sites.

4.3. Thermosondes

[26] A thermosonde is a special type of radiosonde which, in addition to the measurements of pressure, temperature, humidity, etc., also measures with high accuracy (about 10^{-3} K) the variations in temperature over a small horizontal distance (typically around 1 m). These measurements are used to directly estimate the temperature structure constant C_T^2 [*Azouit and Vernin*, 2005]. Unfortunately, similar measurements of the humidity fluctuations are not made; thus, these will not give direct measurements of C_n^2. However,

Table 2. Parameters of Exponential C_n^2 Profiles in Equation (18) for Different Seasons[a]

	Latitude	Longitude	Dec–Feb		Mar–May		Jun–Aug		Sep–Nov	
Station	(°N)	(°E)	C_{n0}^2	H	C_{n0}^2	H	C_{n0}^2	H	C_{n0}^2	H
Lerwick	60	−1	0.7	3301	1.8	2876	1.1	4232	1.9	3114
Herstmonceux	51	0	1.2	2499	4.2	2638	8.5	2659	6.1	2518
Gibraltar	36	−5	4.9	2877	9.3	2964	10.4	3625	13.2	2804
St. Helena	−15	−6	22.5	2257	29.5	1920	20.6	1702	6.6	3207
Mount Pleasant	−52	−58	3.0	3198	2.2	3302	1.4	3224	2.0	2996

[a]C_{n0}^2 and H are in units of 10^{-14} m$^{-2/3}$ and m, respectively.

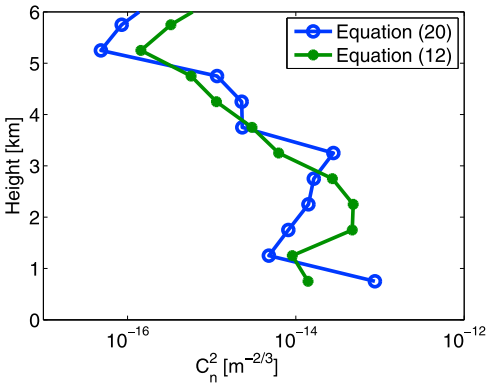

Figure 3. C_n^2 profiles from thermosonde data calculated using equations (12) and (20).

since the temperature structure constant can be described by an expression similar to equation (12) as [*Tatarskii*, 1971]

$$C_T^2 = a^2 F L_0^{4/3} \left[\frac{\partial T}{\partial \theta}\frac{\partial \theta}{\partial z}\right]^2 = a^2 F L_0^{4/3} \left[\left(\frac{P}{P_0}\right)^{0.286}\frac{\partial \theta}{\partial z}\right]^2, \quad (19)$$

we can relate C_T^2 to C_n^2 through

$$C_n^2 = M^2 \left[\left(\frac{P}{P_0}\right)^{0.286}\frac{\partial \theta}{\partial z}\right]^{-2} C_T^2. \quad (20)$$

Hence, we no longer need to estimate L_0 and F since these are embedded in C_T^2. Unfortunately, thermosonde launches are relatively rare.

[27] Figure 3 shows the mean C_n^2 profiles, calculated by equation (20) using C_T^2, pressure, temperature, and humidity profiles recorded by 16 thermosondes launched from Ash Mountain Helibase near Three Rivers, California, during the T-REX campaign from 20 March to 6 April 2006 [*Jumper et al.*, 2007]. For comparison we show the mean C_n^2 profile calculated using equation (12), i.e., in the same way as done for the radiosonde data in section 4.2. We can see that the two methods agree relatively well.

[28] *Zink et al.* [2004] found that C_n^2 profiles estimated from radar and thermosondes agree within a factor of 2 after removing a bias. However, since they used the thermosonde profiles for calibration of the radar measurements, it is not possible to determine any possible bias between the two methods.

4.4. C_n^2 From WVR and GPS Measurements

[29] Measurements of the wet part of the atmospheric delay can also be used to estimate C_n^2. However, since the atmospheric delay is an integrated quantity it is not possible to infer the shape of the C_n^2 profile, so it must be assumed. *Treuhaft and Lanyi* [1987] made the simple assumption that C_n^2 was constant up to an effective tropospheric height H and zero above. They obtained C_n^2 from measurements of the variance of the zenith wet delay ℓ^z over a time period τ:

$$\begin{aligned}\sigma_\ell^2(\tau) &= \frac{1}{\tau^2}\int_0^\tau (\tau - t)\left\langle \left[\ell^z(t+t_0) - \ell^z(t_0)\right]^2\right\rangle dt \\ &= \frac{1}{2\tau^2}\int_0^\tau (\tau - t)\int_0^H\int_0^H \Big[\left\langle \left[n(z,t_0) - n(z',t_0+t)\right]^2\right\rangle \\ &\quad + \left\langle \left[n(z,t_0+t) - n(z',t_0)\right]^2\right\rangle - \left\langle \left[n(z,t_0) - n(z',t_0)\right]^2\right\rangle \\ &\quad - \left\langle \left[n(z,t_0+t) - n(z',t_0+t)\right]^2\right\rangle\Big] dz\, dz'\, dt \\ &= \frac{1}{\tau^2}\int_0^\tau (\tau - t)\int_0^H\int_0^H C_n^2(z,z')\Big[\left((z-z')^2 + v^2t^2\right)^{1/3} \\ &\quad - |z-z'|^{2/3}\Big] dz\, dz'\, dt, \end{aligned} \quad (21)$$

where t_0 denotes the time of the beginning of the time period. Assuming H = 1 km, a mean wind speed of 8 m s^{-1}, and τ = 24 h, they obtained a value of C_n^2 of 5.8×10^{-14} m$^{-2/3}$ using zenith wet delay variances from WVR and radiosonde data. Later work, however, seems to indicate that using H = 2 km is more appropriate [*Linfield and Wilcox*, 1993; *Keihm*, 1995]. This gives $C_n^2 = 1.2 \times 10^{-14}$ m$^{-2/3}$.

[30] Using the same approach, we used the zenith total delay variances over 24 h obtained from GPS data to estimate C_n^2 for the CONT05 and CONT08 campaigns. The GPS data were analyzed with the GIPSY/OASIS-II Software [*Webb and Zumberge*, 1993], and the average of the 1 day variances was calculated for each station. Wind speeds were obtained from ECMWF (at the 850 hPa level). The derived values of C_n^2 are shown in Table 3. We estimated C_n^2 in two ways: By assuming that C_n^2 is constant up to H = 2 km and by using a more realistic model:

$$C_n^2(z,z') = C_{n0}^2 \exp\left[-\frac{z+z'}{H}\right], \quad (22)$$

where we have assumed H = 2 km (approximately the scale height of atmospheric water vapor). For both methods, we calculated one C_n^2 per station per day; then the average C_n^2 for each station was calculated.

[31] *Nilsson et al.* [2005] estimated C_n^2 from variations between slant wet delays of different directions, measured by a WVR. We have used the same method to estimate C_n^2 for the VLBI stations Onsala, Wettzell, and Kokee Park for the CONT05 period (Figure 4). Here we assumed that C_n^2 is constant up to H = 2 km and zero above. We obtain C_n^2 between 10^{-14} and 10^{-13} m$^{-2/3}$ for all three stations. As comparison the time series of C_n^2 estimated from GPS are also shown. As seen there is a good agreement for Onsala while the agreement is worse for Kokee and Wettzell. One reason for this could be that the sampling intervals of the Kokee and Wettzell radiometers are too large (45 s compared to around 10 s for Onsala) for the data to be really useful for estimation of C_n^2.

[32] A method for measuring atmospheric turbulence using data from a local network of GPS receivers was presented by *Nilsson et al.* [2009]. This method was applied to GPS data from the Yucca Mountain Network in Nevada. The results showed a strong seasonal variation in magni-

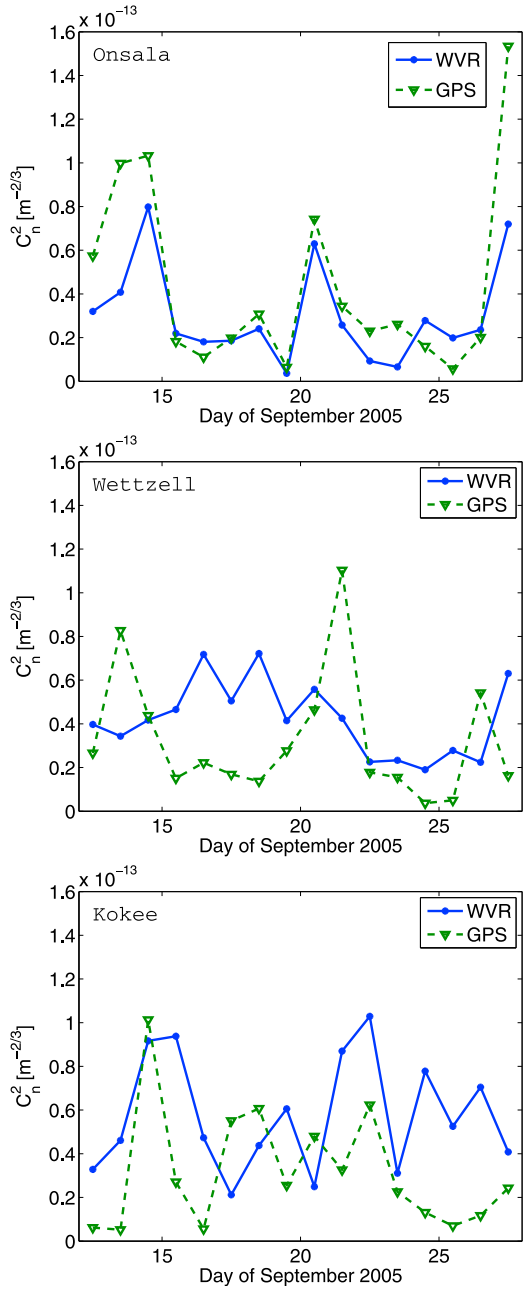

Figure 4. C_n^2 estimated from WVR and GPS data for the CONT05 period at (top) Onsala, (middle) Wettzell, and (bottom) Kokee. The WVRs at Wettzell and Kokee Park are Radiometrics WVR-1100. The Onsala WVR is described by *Elgered and Jarlemark* [1998].

tude of the turbulence, corresponding to a variation in C_n^2 from 0.6×10^{-14} m$^{-2/3}$ in the winter to 4.6×10^{-14} m$^{-2/3}$ in the summer.

4.5. Summary of C_n^2 Measurements

[33] The review shows that C_n^2 is highly variable, both in time and as a function of location. Typically, we can expect the average C_n^2 for most locations to be in the range of 10^{-14}–10^{-13} m$^{-2/3}$ close to the ground and to be decreasing exponentially with height. We expect that C_n^2 is generally larger during warm and humid weather conditions.

5. Simulation Setup and Data Analysis

[34] Assuming that the station positions and velocities, the radio source positions, earth rotation, and orientation are known, and geophysical phenomena (such as solid earth tides, ocean loading, etc.) are modeled accurately, the observed minus the calculated group delay of a VLBI baseline observations can be described as

$$o - c = \ell_1 - \ell_2 + \tau_1 - \tau_2 + w, \tag{23}$$

where ℓ_1 and ℓ_2 are the atmospheric delays for the two stations forming the baseline, τ_1 and τ_2 are the clock errors, and w is the observation noise. Atmospheric delays are simulated using the procedure described in section 3. The observation noise is simulated as white noise with a standard deviation of 30 ps. A clock error is simulated as a random walk process plus an integrated random walk process plus an integrated integrated random walk process. The standard deviations of the driving noise for these processes are 5×10^{-2} ps s$^{-1/2}$, 1×10^{-5} ps s$^{-3/2}$, and 5×10^{-11} ps s$^{-5/2}$, respectively. These are typical values representative for a hydrogen maser (P. Jarlemark, SP Technical Research Institute of Sweden, personal communication, 2008).

[35] The simulated VLBI observations, as well as the actually observed VLBI data, were used in the VLBI analysis software SOLVE [*Ma et al.*, 1990]. For each 24 h period we estimated the station positions (assumed constant over each 24 h period), the clock errors and the atmospheric zenith delays with a 1 h resolution, and the horizontal atmospheric gradients with a 6 h resolution.

6. Results

6.1. Same C_n^2 for All Stations

[36] We first consider the simple case of having the same C_n^2 profile at all stations. We made the simple assumption of a profile constant up to the height $H = 2$ km above ground and zero above. We tested three different values for C_n^2: 10^{-15}, 10^{-14}, and 10^{-13} m$^{-2/3}$. We expect the mean value of C_n^2 over, e.g., 1 day to be approximately 10^{-14}–10^{-13} m$^{-2/3}$ (see section 4).

[37] Figure 5 shows the baseline length repeatabilities obtained from the simulations. The repeatabilities obtained from analysis of the observed data are also shown for comparison. We note that for CONT08 the simulations with $C_n^2 = 10^{-13}$ m$^{-2/3}$ give repeatabilities which are on average similar to the observed ones; that is, the average C_n^2 for CONT08 was probably close to this value. For CONT05 $C_n^2 = 10^{-13}$ m$^{-2/3}$ gives on average too large repeatabilities while $C_n^2 = 10^{-14}$ m$^{-2/3}$ gives too small repeatabilities compared to the observed ones. Thus, the average C_n^2 for CONT05 was probably between 10^{-14} and 10^{-13} m$^{-2/3}$, i.e. smaller than for CONT08. This is reasonable since C_n^2 varies with season, and we expect that it has its maximum value in July-August in the northern hemisphere (in both campaigns, nine of 11 stations are in the northern hemisphere). Fur-

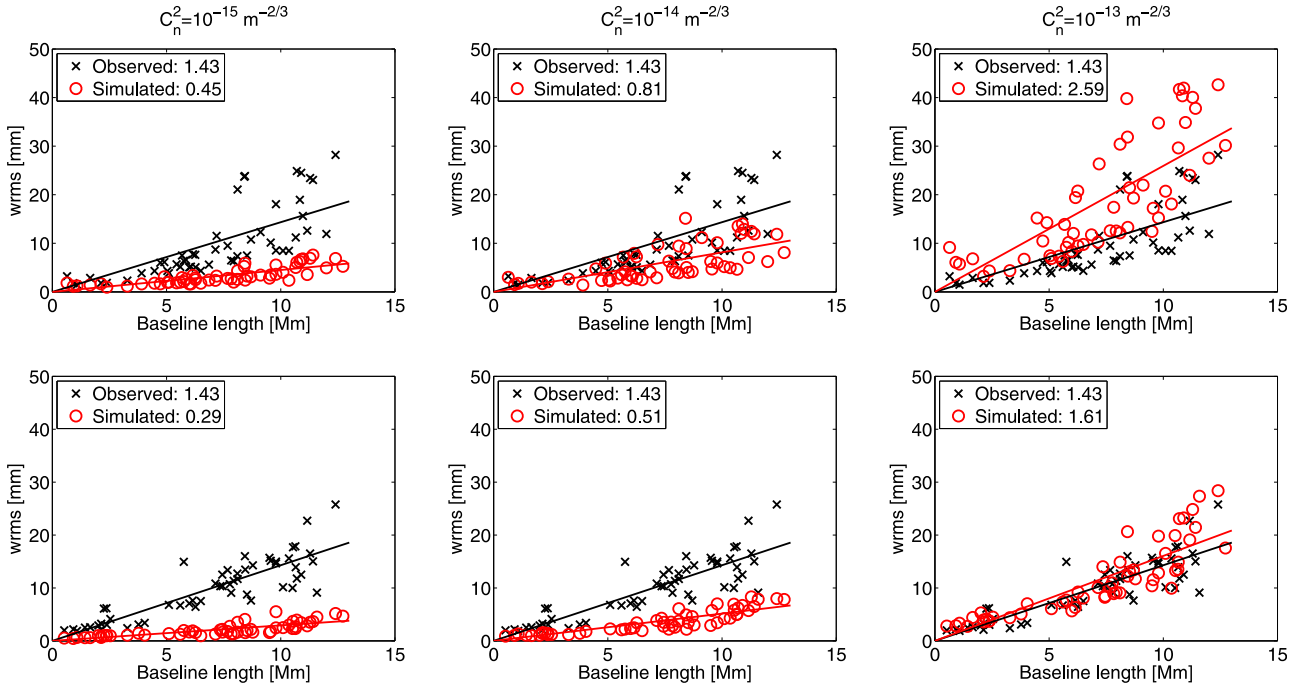

Figure 5. Baseline length repeatabilities obtained from observations (black) and simulations (red) for (top) CONT05 and (bottom) CONT08. The same values for C_n^2 were used for all stations. Also given are the rates (slopes of the straight lines fitted to the data) in mm Mm^{-1} (ppb).

thermore, it is possible that Medicina and Zelenchukskaya (which participated only in CONT08) generally have larger C_n^2 than Algonquin Park and Gilmore Creek (which participated only in CONT05). Especially, we can expect a low C_n^2 at Gilmore Creek since it is located at a high latitude while the other stations are at midlatitudes (see Table 1).

[38] The analysis of the simulations with $C_n^2 = 10^{-15}$ m$^{-2/3}$ gives repeatabilities which are small compared to those obtained from the observed VLBI data. For such a small C_n^2 value, the errors in the VLBI results will mainly be from other error sources (i.e., clock errors and observation noise). Assuming that our simulations of the clock errors and observation noise are realistic (and that all other error sources can be ignored), the fact that the baseline repeatabilities obtained from the analysis of the observed data are much worse than those from the simulated data must be due to a value of C_n^2 that is too low. This shows that atmospheric turbulence is the largest error source for geodetic VLBI today.

6.2. C_n^2 From Radiosonde Data

[39] We simulated atmospheric delays with C_n^2 as described by equation (18) and the model parameters given in Table 2. Unfortunately, the high-resolution radiosonde launch sites for which these parameters were obtained are not close to the VLBI sites that participated in CONT05 and CONT08. Hence, to obtain a C_n^2 profile for a specific VLBI station we used the profile from the radiosonde launch site closest in latitude. For CONT05 we used radiosonde profiles from the September–November period, and for CONT08 we used June–August.

[40] The corresponding baseline length repeatabilities are shown in Figure 6. The repeatabilities from the simulations are generally larger than those from the observed data. There could be several reasons for this. One obvious problem is clearly that the C_n^2 profiles are not obtained close to the VLBI stations. Generally the difference in latitude is less than 10°; however, there could still be large differences in longitude (more than 150° in the worst case; see Tables 1 and 2). It could be that one or more of the radiosonde launch sites are located in a region with unusually high C_n^2. For example, it is known that C_n^2 can be large around and above steep mountains since a lot of turbulence is created when the wind is blowing toward the mountain. The radiosonde launch site at Gibraltar is such an example (we used the C_n^2 from Gibraltar for three VLBI stations). Another possibility is that the method for obtaining C_n^2 from radiosonde data is not accurate enough, since the uncertainty is factor of 2 (see section 4.2).

6.3. C_n^2 From the Variance of Zenith Delays

[41] We also used C_n^2 profiles obtained from the 1 day variances of the zenith total delay estimated from GPS data acquired at the VLBI stations (Table 3). Simulations were made for both profile shapes (constant up to 2 km, and exponential). The baseline length repeatabilities from these simulations are presented in Figure 6.

[42] As seen, the repeatabilities based on these simulations do agree rather well with those obtained from the observed VLBI data. However, for baselines in CONT05 containing Algonquin Park simulations clearly give worse baseline length repeatabilities compared with the observations. The method of using the 1 day variances of the zenith delay may not give realistic C_n^2 values for this station. One reason could be that there are significant nonturbulent variations. However, the method seems to work very well for

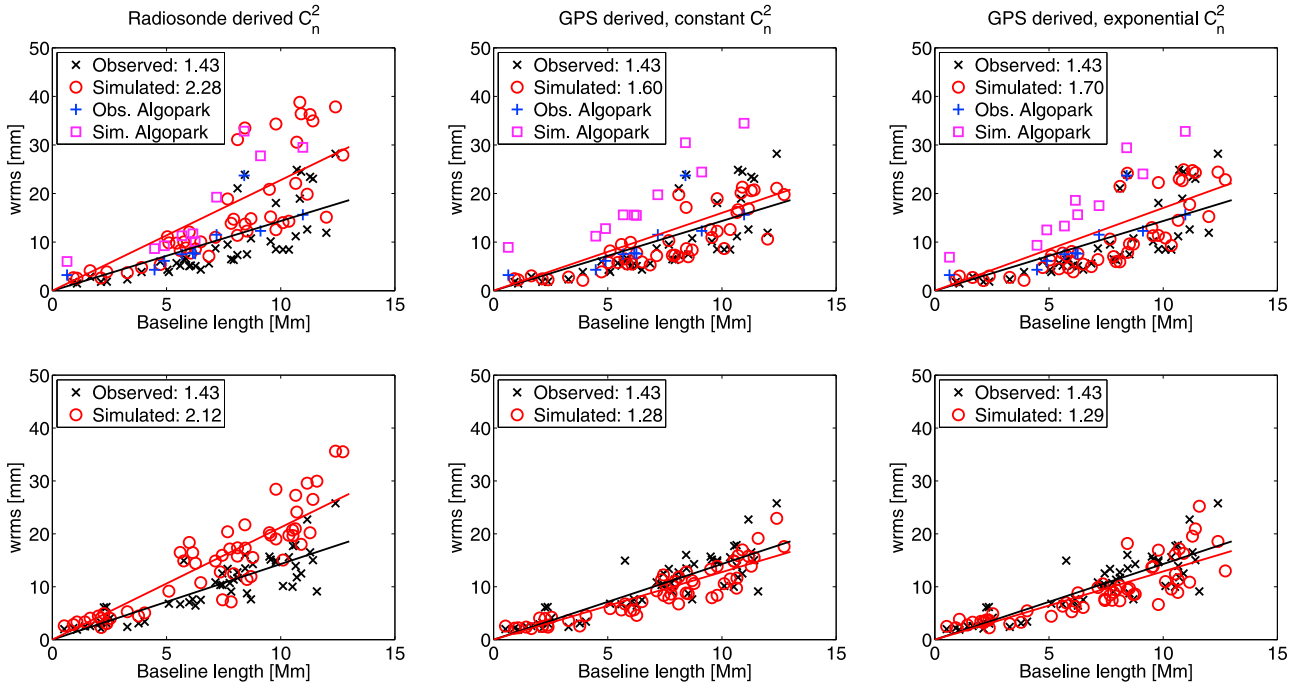

Figure 6. Baseline length repeatabilities obtained from observations (black) and simulations (red) for (top) CONT05 and (bottom) CONT08. The C_n^2 values were obtained (left) from radiosonde data and from zenith total delay variance estimated from GPS data and assuming a (middle) C_n^2 constant up to 2 km and (right) C_n^2 decreasing exponentially with height. Note that for CONT05 and for the simulations with C_n^2 from GPS, the baselines containing Algonquin Park are plotted with different symbols.

the other stations, at least to obtain C_n^2 that can be used in simulations.

[43] We can also note that there are only small differences between using a constant C_n^2 up to 2 km and using a C_n^2 decreasing exponentially with height (equation (22)). This shows that the shape of the C_n^2 is of minor importance for the simulations. It is only important to know the integrated value.

[44] Figure 7 shows the ratios between the baseline length repeatabilities obtained from the analysis of the simulated observations data and the real observations. It can be noted that the ratios are close to 1 for the simulations using the C_n^2 estimated from GPS. For CONT08 the mean values of the ratios are 0.94 and 1.0 for the simulations with C_n^2 constant with height and exponentially decreasing with height, respectively. For CONT05 the corresponding values are 1.3 for both cases. The baselines with Algonquin Park give the largest ratio values. The mean value of the ratios reduces to 1.15 when the baselines with Algonquin Park are excluded.

7. Conclusions and Outlook

[45] The simulations presented indicate that the fluctuations in the atmospheric delays caused by turbulence presently are the largest error source for geodetic VLBI. Thus, in order to improve the accuracy of VLBI results the modeling of the atmosphere needs to be improved in the VLBI analysis and/or the observing strategy needs to be improved.

[46] The simulation of VLBI observations can be a powerful tool to test any new VLBI observing and data analysis strategies. Atmospheric delay simulations using turbulence theory should be implemented into the scheduling software in order to improve and optimize observing schedules. This could easily be done using C_n^2 derived from GNSS data, reflecting, e.g., seasonal C_n^2 variations (section 6.3). The turbulence theory could also be implemented in the data analysis software. For example, the covariance matrix C (equation (5)) can be used to weight the observations.

[47] Another way to improve the VLBI results, even without introducing turbulence theory into the data analysis, is to increase the number of observations. An indication of such an improvement is that the baseline length repeatabilities for CONT08 are smaller than those for CONT05 in the simulations with constant C_n^2. The reason for the improved results is probably due to the fact that more observations with better sky coverage were made in CONT08 (see Table 1). We also note that the baseline repeatabilities for Algonquin Park for the simulations with C_n^2 from GPS are significantly higher than the repeatabilities for other baselines of similar length. This is because the C_n^2 values for Algonquin Park are high (see Table 3), but the number of scans is low (see Table 1). Other stations with high C_n^2 but with more observations, e.g., Westford in CONT05 and Tsukuba in CONT08, are not affected that much. For the observed data the baseline length repeatabilities are similar for CONT05 and CONT08. In this case the accuracy improvement due to more observations was compensated by degradation in accuracy because of higher C_n^2 values (see Table 3 and section 6.1).

[48] The proposed future geodetic VLBI system, VLBI2010 [*Niell et al.*, 2006; *Behrend et al.*, 2008], will consist of radio telescopes with higher slew rates that will be

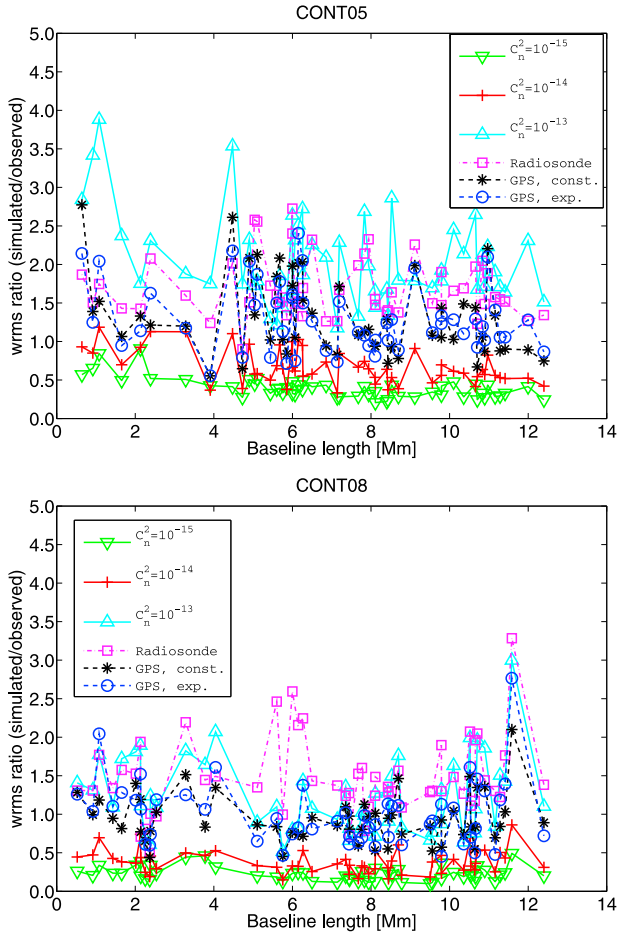

Figure 7. Ratios between baseline length repeatabilities obtained from simulations and from observations. The results are from (top) CONT05 and (bottom) CONT08.

able to make more observations per unit time. The aim of the VLBI2010 system is to reach an accuracy of 1 mm in repeatability for global baselines. The methods presented in this work are currently used in simulations to evaluate whether and how this goal can be reached [see, e.g., *Behrend et al.*, 2008; *MacMillan*, 2008; *Wresnik et al.*, 2008].

[49] In order to do the simulations the structure constant C_n^2 needs to be known. As discussed in section 4, several methods exist to estimate this parameter. The problem is that the instruments used for many of these methods (e.g., radars and high-resolution radiosondes) are not available at very many places and in particular not at VLBI sites. To carry out realistic simulations, we need to know C_n^2 at the VLBI stations. The simulations indicate that the method of estimating C_n^2 from the variance of the zenith total delay has a sufficient accuracy and that the shape of the C_n^2 profile is of minor importance. Time series of the zenith total delay can be obtained from a number of different instruments, such as radiometers, GPS, or even VLBI data. For existing and planned VLBI stations, there are usually GPS stations nearby which can provide time series of zenith total delay for estimation of C_n^2.

[50] The method of simulating atmospheric delays presented in this work could, of course, also be used for simulations of other space geodetic techniques that use radio waves, such as GNSS and Doppler Orbitography and Radiopositioning Integrated by Satellite (DORIS). In principle it should also be possible to use the method for simulating atmospheric delays of optical techniques, such as Satellite Laser Ranging (SRL). It should, however, be noted that C_n^2 for optical wavelengths is generally much lower than for radio waves.

[51] **Acknowledgments.** We are grateful to Gunnar Elgered for his valuable comments on the manuscript. The high-resolution radiosonde data were obtained from the British Atmospheric Data Center (BADC) (http://badc.nerc.ac.uk/data/rad-highres/). Thermosonde data were provided by NCAR/EOL under sponsorship of the National Science Foundation (http://data.eol.ucar.edu/). Wind data were obtained from ECMWF (http://www.ecmwf.int). The CONT05 and CONT08 campaigns were coordinated by the International VLBI Service for Geodesy and Astrometry (IVS) [*Schlüter and Behrend*, 2007]. This work was supported by the Swedish National Space Board.

References

Azouit, M., and J. Vernin (2005), Optical turbulence profiling with balloons relevant to astronomy and atmospheric physics, *Publ. Astron. Soc. Pac.*, *117*, 536–543, doi:10.1086/429785.

Behrend, D., et al. (2008), Recent progress in the VLBI2010 development, in *Observing Our Changing Earth: Proceedings of the 2007 IAG General Assembly, Perugia, Italy, July 2–13, 2007*, *Int. Assoc. Geod. Symp.*, vol. 133, pp., 833–840, doi:10.1007/978-3-540-85426-5, Springer, New York.

Chadwick, R. B., and K. P. Moran (1980), Long-term measurements of C_n^2 in the boundary layer, *Radio Sci.*, *15*(2), 355–361, doi:10.1029/RS015i002p00355.

Cohn, S. A. (1995), Radar measurements of turbulent eddy dissipation rate in the troposphere: A comparison of techniques, *J. Atmos. Oceanic Technol.*, *12*(1), 85–95, doi:10.1175/1520-0426(1995)012<0085:RMOTED>2.0.CO;2.

d'Auria, G., F. S. Marzano, and U. Merlo (1993), Model for estimating the refractive-index stucture constant in clear-air intermittent turbulence, *Appl. Opt.*, *32*, 2674–2680.

Elgered, G. (1993), Tropospheric radio-path delay from ground based microwave radiometry, in *Atmospheric Remote Sensing by Microwave Radiometry*, edited by M. Janssen, pp. 215–258, John Wiley, New York.

Elgered, G., and P. O. J. Jarlemark (1998), Ground-based microwave radiometry and long term observations of atmospheric water vapor, *Radio Sci.*, *33*(3), 707–717, 98RS00488.

Elgered, G., J. L. Davis, T. A. Herring, and I. I. Shapiro (1991), Geodesy by radio interferometry: Water vapor radiometry for estimation of the wet delay, *J. Geophys. Res.*, *95*(B4), 6541–6555, doi:10.1029/90JB00834.

Emardson, T. R., G. Elgered, and J. M. Johansson (1999), External atmospheric corrections in geodetic very-long-baseline interferometry, *J. Geod.*, *73*, 375–383, doi:10.1007/s001900050256.

Heo, B.-H., S. Jacoby-Koaly, K.-E. Kim, B. Campistron, B. Benech, and E.-S. Jung (2003), Use of the Doppler spectral width to improve the estimation of the convective boundary layer height from UHF wind profiler observations, *J. Atmos. Oceanic Technol.*, *20*(3), 408–424, doi:10.1175/1520-0426(2003)020<0408:UOTDSW>2.0.CO;2.

Herring, T. A., J. L. Davis, and I. I. Shapiro (1990), Geodesy by radio interferometry: The application of Kalman filtering to the analysis of very long baseline interferometry data, *J. Geophys. Res.*, *95*(B8), 12561–12,581, doi:10.1029/90JB00683.

Hill, R. J., R. A. Bohlander, S. F. Clifford, R. W. McMillan, J. T. Priestley, and W. P. Schoenfeld (1988), Turbulence-induced millimeter-wave scintillation compared with micrometeorological measurements, *IEEE Trans. Geosci. Remote Sens.*, *26*(3), 330–342.

Hocking, W. K., and P. K. L. Mu (1997), Upper and middle tropospheric kinetic energy dissipation rates from measurements of C_n^2—Review of theories, in situ investigations, and experimental studies using the Buckland Park atmospheric radar in Australia, *J. Atmos. Solar Terr. Phys.*, *59*(14), 1779–1803, doi:10.1016/S1364-6826(97)00020-5.

Jumper, G. Y., J. R. Roadcap, E. A. Murphy, and J. W. Myers (2007), In situ measurements of waves and turbulence in the T-REX campaign, paper presented at 45th AIAA Aerospace Meeting and Exhibit, Am. Inst. of Aeronaut. and Astron., Reno, Nev.

Keihm, S. J. (1995), Water vapor radiometer measurements of the tropospheric delay fluctuations at Goldstone over a full year, *Telecommun. Data Acquisition Prog. Rep. 42-122J*, pp. 1–11, NASA, Washington, D. C.

Kuehn, C. E., W. E. Himwich, T. A. Clark, and C. Ma (1991), An evaluation of water vapor radiometer data for calibration of the wet path delay in very long baseline interferometry experiments, *Radio Sci.*, *26*(6), 1381–1391, doi:10.1029/91RS02020.

Linfield, R. P., and J. Z. Wilcox (1993), Radio metric errors due to mismatch and offset between a DNS antenna beam and the beam of a tropospheric calibration instrument, *Telecommun. Data Acquisition Prog. Rep. 42-114A*, pp. 1–13, NASA, Washington, D. C.

Luce, H., M. Crochet, F. Dalaudier, and C. Sidi (1997), An improved interpretation of VHF oblique radar echoes by a direct balloon C_n^2 estimation using a horizontal pair of sensors, *Radio Sci.*, *32*(3), 1261–1268, doi:10.1029/97RS00053.

Ma, C., J. M. Sauber, L. J. Bell, T. A. Clark, D. Gordon, W. E. Himwich, and J. W. Ryan (1990), Measurement of horizontal motions in Alaska using very long baseline interferometry, *J. Geophys. Res.*, *95*(B13), 21991–22,011, doi:10.1029/JB095iB13p21991.

MacMillan, D. S. (1995), Atmospheric gradients from very long baseline interferometry observations, *Geophys. Res. Lett.*, *22*(9), 1041–1044, doi:10.1029/95GL00887.

MacMillan, D. S. (2008), Simulation analysis of the geodetic performance of networks of VLBI2010 stations, in *Measuring the Future: Proceedings of the 5th IVS General Meeting*, edited by A. Finkelstein and D. Behrend, pp. 416–420, Inst. of Appl. Astron., St. Petersburg, Russia.

Nastrom, G. D., K. S. Gage, and W. L. Ecklund (1986), Variability of turbulence, 4–20 km, in Colorado and Alaska from MST radar observations, *J. Geophys. Res.*, *91*(D6), 6722–6734, doi:10.1029/JD091iD06p06722.

Niell, A. (1996), Global mapping functions for the atmosphere delay at radio wavelengths, *J. Geophys. Res.*, *101*(B2), 3227–3246, doi:10.1029/95JB03048.

Niell, A., A. Whitney, B. Petrachenko, W. Schlüter, N. Vandenberg, H. Hase, Y. Koyama, C. Ma, H. Schuh, and G. Tuccari (2006), VLBI2010: Current and future requirements for geodetic VLBI systems, in *IVS 2005 Annual Report*, edited by D. Behrend and K. Baver, *NASA Tech. Publ., NASA TP-2006-214136*, 13–40.

Nilsson, T., and R. Haas (2008), Modeling tropospheric delays with atmospheric turbulence model, in *Measuring the Future: Proceedings of the 5th IVS General Meeting*, edited by A. Finkelstein and D. Behrend, pp. 361–370, Inst. of Appl. Astron., St. Petersburg, Russia.

Nilsson, T., L. Gradinarsky, and G. Elgered (2005), Correlations between slant wet delays measured by microwave radiometry, *IEEE Trans. Geosci. Remote Sens.*, *43*(5), 1028–1035, doi:10.1109/TGRS.2004.840659.

Nilsson, T., R. Haas, and G. Elgered (2007), Simulations of atmospheric path delays using turbulence models, in *Proceedings of 18th European VLBI for Geodesy and Astrometry (EVGA) Working Meeting*, edited by J. Böhm, A. Pany, and H. Schuh, pp. 175–180, Vienna Univ. of Technol., Vienna, Austria.

Nilsson, T., J. L. Davis, and E. M. Hill (2009), Using ground-based GPS to characterize atmospheric turbulence, *Geophys. Res. Lett.*, *36*, L16807, doi:10.1029/2009GL040090.

Ottersten, H. (1969), Radar backscattering from the turbulent clear atmosphere, *Radio Sci.*, *4*(12), 1251–1255, doi:10.1029/RS004i012p01251.

Press, W. H., S. A. Teukolsky, W. T. Vetterling, and B. P. Flannery (1992), *Numerical Recipes in FORTRAN: The Art of Scientific Computing*, 2nd ed., Cambridge Univ. Press, Cambridge, U. K.

Rao, D. N., P. Kishore, T. N. Rao, S. V. B. Rao, K. K. Reddy, M. Yarraiah, and M. Hareesh (1997), Studies on refractivity structure constant, eddy dissipation rate, and momentum flux at a tropical latitude, *Radio Sci.*, *32*(4), 1375–1389, doi:10.1029/97RS00251.

Rao, D. N., T. N. Rao, M. Venkataratnam, S. Thulasiraman, S. V. B. Rao, P. Srinivasulu, and P. B. Rao (2001), Diurnal and seasonal variability of turbulence parameters observed with Indian mesosphere-stratosphere-troposphere radar, *Radio Sci.*, *36*(6), 1439–1457, doi:10.1029/2000RS002316.

Ravard, O., and F. Chevrier (1996), Volume scattering by tropospheric turbulence at midlatitudes: Frequency validity range, *Radio Sci.*, *31*(4), 821–831, doi:10.1029/96RS00434.

Schlüter, W., and D. Behrend (2007), The international VLBI Service for Geodesy and Astrometry (IVS): Current capabilities and future prospects, *J. Geod.*, *81*(6–8), 379–387, doi:10.1007/s00190-006-0131-z.

Tatarskii, V. I. (1971), *The Effects of the Turbulent Atmosphere on Wave Propagation*, Isr. Program for Sci. Transl., Jerusalem.

Taylor, G. I. (1938), The spectrum of turbulence, *Proc. R. Soc. London, Ser. A*, *164*(919), 476–490.

Treuhaft, R. N., and G. E. Lanyi (1987), The effect of the dynamic wet troposphere on radio interferometric measurements, *Radio Sci.*, *22*(2), 251–265, doi:10.1029/RS022i002p00251.

VanZandt, T. E., J. L. Green, K. S. Gage, and W. L. Clark (1978), Vertical profiles of refractivity turbulence structure constant: Comparison of observations by the Sunset Radar with a new theoretical model, *Radio Sci.*, *13*(5), 819–829, doi:10.1029/RS013i005p00819.

Vasseur, H. (1999), Prediction of tropospheric scintillation on satellite links from radiosonde data, *IEEE Trans. Antennas Propag.*, *47*(2), 293–301, doi:10.1109/8.761069.

Webb, F. H., and J. F. Zumberge (1993), An introduction to the GIPSY/OASIS-II, *JPL Publ. D-11088*, Jet Propul. Lab., Pasadena, Calif.

Wresnik, J., J. Boehm, A. Pany, and H. Schuh (2008), VLBI2010 simulations at IGG Vienna, in *Proceedings of the 5th IVS General Meeting: Measuring the Future*, edited by A. Finkelstein and D. Behrend, pp. 421–426, Inst. of Appl. Astron., St. Petersburg, Russia.

Zink, F., R. A. Vincent, E. Murphy, and O. Cote (2004), Comparison of radar and in situ measurements of atmospheric turbulence, *J. Geophys. Res.*, *109*, D11108, doi:10.1029/2003JD003991.

R. Haas, Onsala Space Observatory, Department of Radio and Space Science, Chalmers University of Technology, SE-439 92 Onsala, Sweden. (rudiger.haas@chalmers.se)

T. Nilsson, Institute of Geodesy and Geophysics, Vienna University of Technology, Gusshausstrasse 27-29, A-1040 Vienna, Austria. (tobias.nilsson@tuwien.ac.at)